European Radiology (2019) 29:6559–6570
https://doi.org/10.1007/s00330-019-06224-6

COMPUTED TOMOGRAPHY

Diagnostic performance of dual-energy CT and subtraction CT for renal lesion detection and characterization

Ali Pourvaziri[1] · Anushri Parakh[1] · Amirkasra Mojtahed[1] · Avinash Kambadakone[1] · Dushyant Vasudeo Sahani[2]

Received: 15 January 2019 / Revised: 21 March 2019 / Accepted: 4 April 2019 / Published online: 27 May 2019

Abstract

Purpose To compare the effect of dual-energy CT (DECT) material density datasets on diagnostic performance, readers' confidence, and interpretation time for renal lesion detection and characterization in comparison to subtraction CT (SCT).

Material and methods One hundred fourteen patients (69/45 = M/F, mean age = 67 years) who underwent contrast-enhanced DECT between January 2015 and February 2018 for suspected renal mass were included retrospectively. For each patient, three radiologists assessed three image datasets: group A, material density iodine (MDI) + material density water (MDW); group B, SCT only; and group C, SCT + true unenhanced phase + virtual monochromatic images at 65 keV. Readers evaluated image quality (4-point scale), the number of lesions, and likely diagnosis. Reading times were recorded. Quantitatively, iodine concentration (IC from MDI) and delta Hounsfield units (ΔHU) for all lesions were measured. Diagnostic accuracy was compared using the area under the receiver operating characteristic curve (AUC). Image quality and interpretation time were compared with Kruskal-Wallis and *t* tests.

Results Study cohort (230 lesions; mean size = 23.63 mm (5–116 mm)) consisted of 60 enhancing, 158 non-enhancing, and 12 lipid-dominant angiomyolipoma lesions. Significantly higher image quality was demonstrated for MDI compared to SCT (mean score = 3.82 vs. 3; $p < 0.05$). Comparable diagnostic accuracy was observed for group A (AUC = 0.88) and group C (AUC = 0.87) and was higher compared to that for group B (AUC = 0.75). Group A was read faster than group C (41.49 s vs. 71.45 s per exam; $p < 0.05$). Both IC and ΔHU values had high accuracy (AUC = 0.97) for differentiating enhancing vs. non-enhancing lesions; however, IC enabled differentiation of clear cell renal cell carcinoma from other enhancing lesions with moderate accuracy (AUC = 0.73).

Conclusion MDI images increase readers' confidence for renal lesion detection and characterization while providing a more efficient radiologist workflow, irrespective of readers' experience.

Key Points

- *Material density iodine (MDI) images enable faster interpretation due to high image quality and potentially reduced need for quantitation.*
- *MDI images increase diagnostic confidence of readers, irrespective of radiologists' experience.*
- *High accuracy with dual-energy CT (DECT) can potentially reduce healthcare costs by eliminating the need for additional investigations.*

Keywords Kidney · X-ray computed tomography · Workflow · Neoplasms · Radiologist

✉ Dushyant Vasudeo Sahani
dsahani@uw.edu

[1] Department of Radiology, Division of Abdominal Imaging and Intervention, Massachusetts General Hospital, Harvard Medical School, 55 Fruit St, White 270, Boston, MA 02114, USA

[2] Department of Radiology, University of Washington, Box 357115, Seattle, WA 98195-7115, USA

Abbreviations

AUC	Area under the receiver operating characteristic curve
cRCC	Clear cell renal cell carcinoma
DECT	Dual-energy CT
dsDECT	Dual-source dual-energy CT
IC	Iodine concentration
IQ	Image quality

MDI	Material density iodine
MDW	Material density water
NIC	Normalized iodine concentration
R-CT	Multiphasic renal mass protocol with conventional CT
ROC	Receiver operating characteristic
ROI	Region of interest
rsDECT	Rapid kV-switching dual-energy CT
SCT	Subtraction CT
TS	Tuberous sclerosis
TUE	True unenhanced
PACS	Picture archiving and communication system
RCC	Renal cell carcinoma
SECT	Stimulated single-energy CT

Introduction

The incidence of renal lesions has been rising steadily [1–3]. As many as 30% of patients over the age of 50 have at least one incidental renal lesion on imaging [4]. Although a majority of these incidental lesions are benign on initial evaluation, up to 12% require further workup. Subsequently, up to two thirds of renal cancers are now discovered incidentally [5].

In most centers, multiphasic renal mass protocol with conventional CT (R-CT) is the preferred next method to characterize renal lesions. R-CT has been extensively validated through collective experience for acceptance in routine clinical settings. It offers ease of use, good image quality, and enhancement quantification benefits [6]. However, it is not without shortcomings and despite the additional cost of exam and concerns for radiation dose and contrast media use, R-CT may fail to characterize up to 7–17% of small renal lesions [7]. Furthermore, it can be affected by beam hardening artifact, pseudo-enhancement, lack of proper contrast timing, and variability in Hounsfield units (HU) [8–10]. These limitations lead to additional interventions, investigations, and an increase in healthcare cost [11, 12].

Subtraction software is a technique to overcome these challenges and has been applied on R-CT images (subtraction CT (SCT)). By subtracting contrast enhancement phase from non-contrast baseline images, it has shown to improve assessment of enhancement and improve readers' confidence [13–16].

Dual-energy CT (DECT) is another technique that offers several potential benefits for renal lesion detection and characterization [17–19]. Material density iodine (MDI) image reconstruction from DECT provides material-specific information to improve lesion enhancement conspicuity with minimal constraints of beam hardening artifacts and pseudo-enhancement [17, 20, 21]. Studies have confirmed the role of DECT to improve renal lesion characterization. We postulated that the high image quality and robustness of MDI images might result in an efficient characterization of renal lesions from reviewing fewer image datasets. It might also offer higher confidence to readers and, hence, rely less on readers' expertise. Thus, the aim of this study is to compare DECT material density datasets to SCT in regard to diagnostic performance, readers' confidence, and interpretation time.

Material and methods

Institutional review board approval was obtained for this retrospective, HIPAA-compliant study, and it waived the requirement for informed consent.

Study cohort

We retrospectively searched our database (Radimetrics, Bayer Healthcare) to identify subjects who underwent multiphasic upper abdominal CT on a rapid kV-switching DECT (rsDECT) scanner for a suspected renal mass between January 2015 and February 2018. The inclusion criteria were as follows: (a) patients scanned with renal mass protocol DECT and (b) availability of processed images for MDI and material density water (MDW) (surrogate of virtual unenhanced exam) and subtraction images. CT exams with the following criteria were excluded from our study: (a) those who did not follow inclusion criteria and had only some or part of the processed images ($n = 14$), (b) those without adequate standard of reference data ($n = 73$), (c) those that were subsequently found to have no renal lesions ($n = 15$), and (d) lesions treated with locoregional therapy or biopsy ($n = 2$) (Fig. 1).

CT technique and image reconstruction

All CT scans were performed on a single-source 64-channel scanner with rsDECT technology (Discovery CT750 HD scanner, GE Healthcare). The renal mass protocol of true unenhanced (TUE) phase was acquired in single-energy CT, followed by nephrographic phase acquired in dual-energy mode.

The scan coverage was limited to the abdomen, extending from the top of kidneys to the iliac crest. The acquisition parameters are listed in Table 1. The scan length and slice thickness were kept similar and acquired at end expiration for both phases to generate the SCT series. All patients received 80–120 ml weight-adapted non-ionic intravenous iodinated contrast medium (Isovue 370; Bracco Diagnostics; less than 135 lb = 80 ml, 136–200 lb = 90 ml, and 201–250 lb = 120 ml). Nephrographic phase acquisition was performed at a fixed delay of 100 s after the start of injection.

The following DECT image datasets were reconstructed and sent to picture archiving and communication system (PACS) for diagnostic interpretation: (a) TUE images (2.5 mm); (b) 140-kVp-equivalent *quality check* of nephrographic phase (2.5 mm); (c) MDI and MDW images

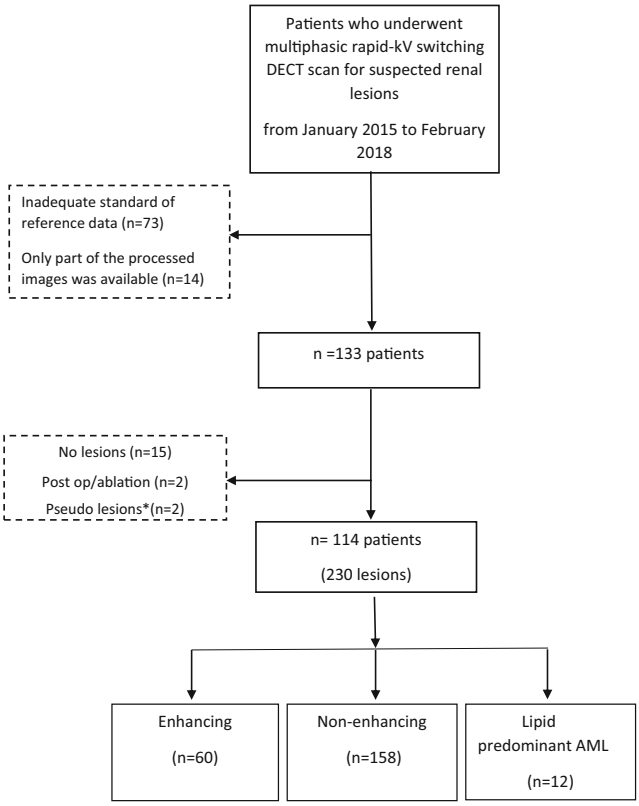

Fig. 1 Flow chart depicting patient selection

(2.5 mm), all of which were in axial plane; and (d) 65-keV monoenergetic images in the nephrographic phase in axial (2.5 mm), coronal (3 mm), and sagittal (3 mm) planes. In addition, the SCT series was reconstructed on the scanner console by the operating CT technologist using a vendor-neutral software program which performs pixel-wise subtraction of TUE phase from the 65-keV dataset, and the resultant SCT series (2.5 mm) was sent to PACS.

Image interpretation

Qualitative image analysis was performed independently by three board-certified radiologists specialized in abdominal imaging (R1 = 18 years; R2 = 9 years; R3 = 3 years) on a PACS workstation in a blinded fashion. To minimize recall bias, the interpretation was carried out in two separate sessions a minimum of 2 weeks apart.

Reading sessions and lesion selection

In session 1 (group A), readers rendered interpretation on DECT material density images: MDI followed by MDW. In session 2, readers first interpreted SCT (group B) followed by a combination of TUE phase and 65-keV monoenergetic nephrographic phase images in three planes (group C). Lesions less than 5 mm were not included. Readers subjectively assessed whether lesions between 5 and 10 mm were too small for characterization in order to maintain consistency with routine practice. These lesions were only included for qualitative assessment (detection and readers' ability to characterize). Due to the lack of reference of standard and inaccurate measurement for lesions of this size [9], they were excluded from our final cohort and assessment of diagnostic accuracy. In patients with multiple lesions, a maximum of five lesions per subject was analyzed. In these patients, the readers were instructed to prioritize enhancing lesions followed by lesions with the largest dimensions.

Qualitative analysis

Reading sessions were conducted based on a pre-designed standardized format (Fig. 2). In each session, the readers first (A) assessed image quality (IQ) on a 4-point Likert scale: (1) worst quality-unacceptable, no diagnosis is possible; (2) sub-optimal quality, diagnostic confidence is reduced but possibly sufficient for diagnosis; (3) good image quality, where minor artifacts do not interfere with the lesion interpretation; and (4) excellent image quality, without artifacts, with minimal to no perceived noise; then, (B) each lesion was categorized as enhancing or non-enhancing and subsequently characterized as (1) solid enhancing, (2) cystic with nodular enhancement, (3) cystic with thin septa, (4) hyperdense cyst, or (5) simple cyst. Categories 1 and 2 were considered enhancing, and categories 3–5 were considered non-enhancing. The presence or absence of fat was also noted. Thereafter, (C) the level of diagnostic confidence for each lesion was indicated on a 4-point Likert scale (1 = not confident; 2 = minimally confident; 3 = somewhat confident; 4 = fully confident). For group A, change in interpretation (lesion category or diagnostic confidence) after the addition of MDW was also recorded. In session 2, for group C, we tried to simulate routine clinical practice and readers had the freedom to place regions of interest (ROIs) as needed and review all the datasets except MDI and MDW (Fig. 2).

An independent reviewer, not part of the reader pool, recorded the time taken by the readers for qualitative image analysis using a stopwatch for each session (sessions 1 and 2). The independent reviewer also recorded the number of times the readers performed ROI evaluation on the images for assessment of lesion density or enhancement.

Quantitative analysis

Quantitative analysis was performed on PACS by another radiologist (AP, with 5 years of experience) who did not perform the qualitative analysis. The number and size of lesions were recorded for all subjects. For all lesions, the largest possible ROIs were placed on TUE phase, 65-keV images for HU increase (ΔHU) and MDI for iodine concentration (mg/ml). In addition, an ROI was placed in the aorta on MDI images at L1 level for obtaining iodine concentration (IC). Normalized

Table 1 Scan protocol for the renal mass DECT acquisition

Scan parameters	True unenhanced phase	Nephrographic phase
Tube voltage (kVp)	120	80/140
Tube current (mA)	Automatic tube current modulation[a]	No tube current modulation
	< 150 lb, 150–350	< 150 lb, 630
	> 150 lb, 150–450	> 150 lb, 600
Noise index	< 150 lb, 20 > 150 lb, 22	
Rotation time (s)	0.5	< 150 lb, 0.5
		> 150 lb, 0.8
DLP (mGy-cm) mean ± standard deviation	334.83 ± 117.01	630.66 ± 161.93
$CTDI_{vol}$ (mGy) mean ± standard deviation	9.33 ± 2.73	18.58 ± 1.51
Pitch	1.375	
ASIR	50%	
Slice thickness/interval	2.5/2.5 mm	
Reconstruction kernel	Standard soft tissue	
Scanner detector configuration	64 × 0.625	
Field of view	500 mm	
Matrix size	512 × 512	
Voxel size	0.98 mm × 0.98 mm × 2.5 mm	

ASIR adaptive statistical iterative reconstruction

[a] These values represent the min/max

iodine concentration (NIC) was computed by obtaining a ratio of lesion to aortic iodine concentrations to negate scan time and hemodynamic variations.

Reference of standard

Enhancing renal mass is identified by the HU difference of 20 (ΔHU > 20) between non-contrast and 65-keV monochromatic image dataset. Non-enhancing lesions were defined as the HU difference less than 10 HU. Lesions that were not fitted to the above criteria (ΔHU = 10–20) were characterized per constellation of findings from additional imaging, clinical history, or pathology. Non-enhancing lesions which measured > 20 HU on non-contrast imaging were considered hyperdense lesions. Cystic lesions were classified in accordance with the Bosniak classification system. Bosniak 3 and 4 lesions were considered to be enhancing, and Bosniak 1, 2, and 2f lesions were considered to be non-enhancing. Lesions that showed macroscopic fat without calcification were considered as lipid-dominant AMLs. These lesions were easily discovered by the presence of macroscopic fat, so lesions' level of enhancement was not of significance; hence, we exclude them from qualitative and quantitative analyses. In lesions without histopathology confirmation, classifications were confirmed by another imaging or follow-up with a minimum of 6 months apart or histopathology. Details of the lesions' demographics and size and how they are identified are depicted in Table 2.

Statistical analysis

For qualitative assessment, the comparison of image quality among groups was performed with the Kruskal-Wallis test. Statistical analyses were conducted using GraphPad Prism (version 6 for Mac; GraphPad Software). Comparison of the interpretation times between sessions was conducted with *t* test using SPSS (version 22). For comparison between confidence means between three groups (A, B, and C), post hoc analysis of variance was performed (SPSS). For comparison of small lesion detection rate, chi-square test was performed (SPSS). To measure the agreement between three readers, the Fleiss kappa test was performed using Stata (version 15; Stata Corp.). Conventionally, a kappa value of lower than 0.20 is considered to be of poor agreement; between 0.21 and 0.40, fair; between 0.41 and 0.60, moderate; and between 0.61 and 0.80, substantial; finally, a value greater than 0.80 is considered to be almost of perfect agreement. To account for clustered correlations in the tri-reader analysis, overall diagnostic performance for all groups was estimated based on binary logit–modeled receiver operating characteristic (ROC) curves using the generalized estimating equation approach with SAS software (PROC NLMIXED SAS v9). To build our binary model for ROC curve analysis, we considered non-enhancing lesion as true negative (TN) and enhancing lesions as true positives (TPs). To evaluate the accuracy of quantitative parameters for lesion discrimination, ROC curve analysis was performed, and the Youden index was used to select a

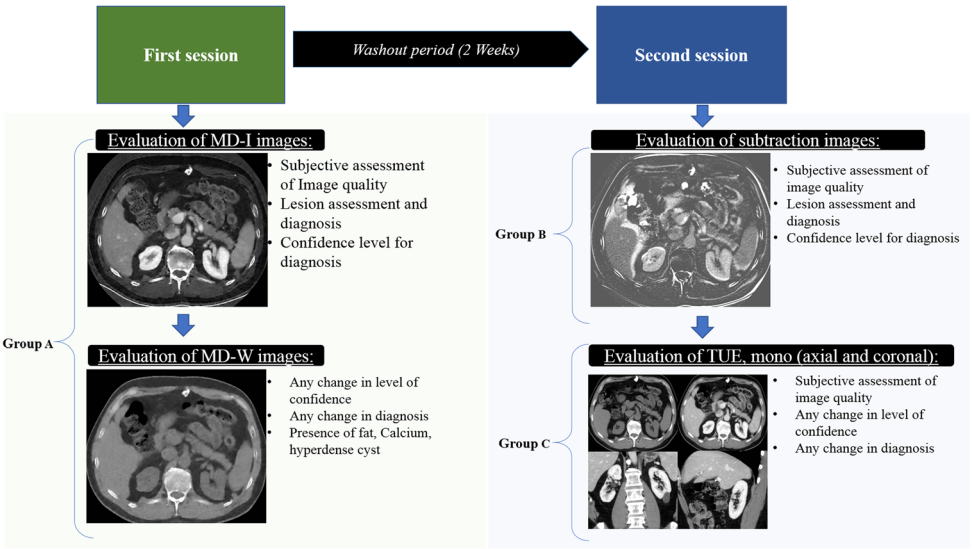

Fig. 2 Flow chart depicting subjective image analysis by readers of study design

suitable threshold. A p value of < 0.05 was considered statistically significant.

Results

Our final cohort consisted of 114 subjects (69 males and 45 females, mean age = 67.24 years, range = 24–93). A total of 230 lesions (mean size = 23.63 mm, range = 5–116 mm) were found with an average of 2.06 lesions per patient. Based on our reference of standard, 60 were characterized as enhancing. Among the enhancing lesions, 30 had pathological confirmation (20 renal cell carcinomas (RCCs), 4 AMLs, 4 oncocytomas, 1 metastasis, and 1 normal renal parenchyma). Fifteen were lipid-poor AMLs in tuberous sclerosis (TS) patients, and 15 were enhancing masses that were under surveillance due to patients' age (mean = 78.76 years, range = 61–91 years), size of the lesions (mean = 19.3 mm, range = 10–46.7 mm), and patients' preferences. One hundred fifty-eight non-enhancing lesions consisted of simple cysts or cysts with thin septation ($n = 113$, 66 patients, 46 males, 20 females, mean age = 69.8) and hyperdense cysts ($n = 45$, 32 patients, 21 males, 11 females, mean age = 68.12 years). Details of the lesions' demographics and size and how they are identified are depicted in Table 2.

Qualitative analysis

Image quality and reader's confidence

All readers reported significantly higher IQ values for group A (MDI and MDW groups, pooled mean = 3.82, SD = 0.45) and group C (stimulated single-energy CT (SECT) sessions, pooled mean = 3.95, SD = 0.23) than group B (SCT, pooled mean = 3, SD = 0.79) (p value = 0.001). There was no statistically significance difference between IQ scores of groups A and B (p value = 0.05). Misregistration artifact in SCT (group B) led to a lower score in IQ assessment. IQ scores mirrored the reader's confidence, and readers had significantly higher confidence scores in group A (p value < 0.05) (Fig. 3).

Diagnostic performance

There was a high agreement between three readers in all groups (group A, 0.71; group B, 0.72; group C, 0.72; p value < 0.05 for all groups). The numbers of lesions that were missed or considered too small for characterization by readers are listed (Table 3). Overall, fewer lesions were considered too small to characterize or missed in group A (0.99%) compared to group B (10.35%) and group C (3.54%) (p value < 0.05).

The area under the receiver operating characteristic curve (AUC) for overall diagnostic accuracy of the three groups is as follows: AUC = 0.8854 (95% CI = 0.8560–0.9147) for group A, AUC = 0.7515 (95% CI = 0.7117–0.7912) for group B, and AUC = 0.8748 (95% CI = 0.8460–0.9036) for group C. The diagnostic performance of group A was significantly better than that of group B ($p < 0.05$), but not significantly different than that of group C (Fig. 4).

The performance accuracy of three readers on single-acquisition MDI and MDW was similar to the renal mass city protocol and higher than subtraction CT.

In group A, three readers misclassified 8–14 lesions. Between 5 and 9 non-enhancing lesions were classified as enhancing (FP), and 3–5 enhancing lesions were classified as non-enhancing (FN). In group B, 17–25 lesions were misclassified, of which 5–7 were non-enhancing (FP) and 12–18 were enhancing (FN). In group C, 11–19 lesions were misclassified, of which 5–14 were non-enhancing (FP) and 5–7 were enhancing (FN). Lesions that were false positives and negatives were potentially due to small size (< 20 mm) and

Table 2 Patient and lesion characteristics and methods of confirmation

	Characteristics							
	Non-enhancing		Enhancing					Miscellaneous lesions
	Simple cyst[a]	Hyperdense cyst	RCC[b]	Lipid poor angiomyolipoma	Oncocytoma	Enhancing mass under surveillance	Other[c]	Lipid predominant AML
No. of lesions	113	45	20	19	4	15	2	12
Size of lesion (mm)	26.7[d] (5–89)	15.42 (5–63)	29.12 (9.2–92)	27.396 (11.4–65)	29.05 (21–33.5)	19.3 (10–46.7)	13.9 (13–14.8)	13.74 (6.5–18)
Patient demographics								
Number of patients	66	32	20	8	4	13	2	11
Gender (F/M)	20/46	11/21	5/15	4/4	1/3	9/4	9/4	10/1
Age (years)	69.8 (93–35)	68.12 (88–46)	67 (49–75)	43.62 (21–77)	76.5 (93–54)	78.76 (61–91)	–	71 (53–86)
Method of confirmation								
Follow-up days from DECT and the additional modality used (per lesion)	1166.42 (132–4970) CT = 73 MR = 22 US = 18	979.91 (214–1238) CT = 35 MR = 5 US = 3	N/A	1463 (658–2991) CT = 5 MR = 10	N/A	816.3 (233–3348) CT = 11 MR = 4	N/A	N/A
Histopathology	N/A	2	20	4	4	N/A	2	N/A
Presence of fat without calcification Diagnosed tuberous sclerosis	N/A	N/A	N/A	Tuberous sclerosis = 15	N/A	N/A	–	Presence of macroscopic fat = 12

[a] Includes simple cyst without septations and cysts with thin septa without measurable enhancement

[b] Clear cell = 12, papillary = 6, clear cell papillary = 1, not classified = 1

[c] Two lesions were biopsy-proven metastasis from non-small cell lung carcinoma and normal parenchyma

[d] Data are presented as mean and range (in parentheses)

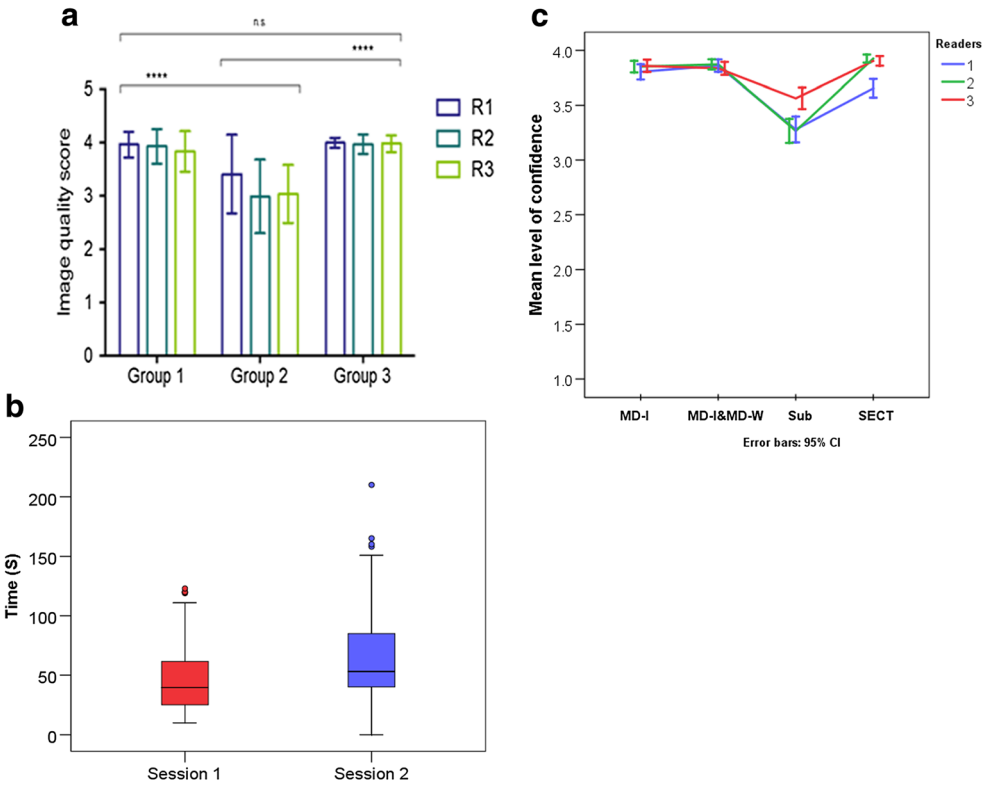

Fig. 3 **a** Means of subjective image quality assessment. **b** Means of level of confidence for each group. **c** Interpretation time in each session and their corresponding SDs. ****p value < 0.05

hyperdense in attenuation, were subtly enhancing, or had complex septal enhancement. Misregistration artifact was a potential cause of misclassification in group B.

MDW

Virtual unenhanced images (MDW) were useful in characterizing 7.23% of lesions (51 lesions out of 705 in all three readers). They increased the level of confidence in characterization of 3.97% of lesions (23 out of 705, pooled lesions of all readers) and changed the classification in 3.26% (28 out of 705). The changes in diagnosis were as follows: change to hyperdense cysts ($n = 20$), discerning fat ($n = 4$), change the lesion from non-enhancing to enhancing ($n = 3$), and change the lesion from enhancing to non-enhancing ($n = 1$).

Table 3 Numbers of lesions that were considered too small for characterization or missed

	Group A		Group B		Group C	
	Too small	Missed	Too small	Missed	Too small	Missed
Reader 1	0	1	6	20	5	4
Reader 2	2	0	10	15	7	2
Reader 3	2	2	7	15	4	3
Total	4	3	23	50	16	9

Small lesions

Forty-two lesions measured 5–10 mm. In this subset of small lesions, readers were not able to characterize 16.6% of lesions in group C ($n = 21$, a pooled number of small lesions among all readers, of which 16 were considered too small and 5 were missed), while in group A, only 7.9% of lesions were not evaluated ($n = 8$ were considered too small, $n = 2$ were missed) (p value < 0.05). Readers could accurately characterize lesions as small as 5 mm in group A, while the smallest lesion that was confidently characterized in group C was 6.5 mm.

Time to interpretation

The mean time for interpreting in session 1, for interpreting MDI and MDW datasets, was 42% lower than that in session 2, for interpreting subtraction datasets and SECT image datasets (41.49 s vs. 71.45 s; p value < 0.05) (Fig. 3c).

Results from qualitative assessment suggest that the accuracy of group A dataset (MDI and MDW) is superior to SCT and comparable to group C dataset (simulated SECT images) while reviewing fewer datasets. As illustrated, readers were more confident (level of confidence is equal to 4 in group A vs. 3 in group B) and faster (41.49 s in session 1 vs. 71.45 s in session 2) and tended to characterize a greater number of small lesions (7.9% vs. 16.6%). MDW images were only needed in

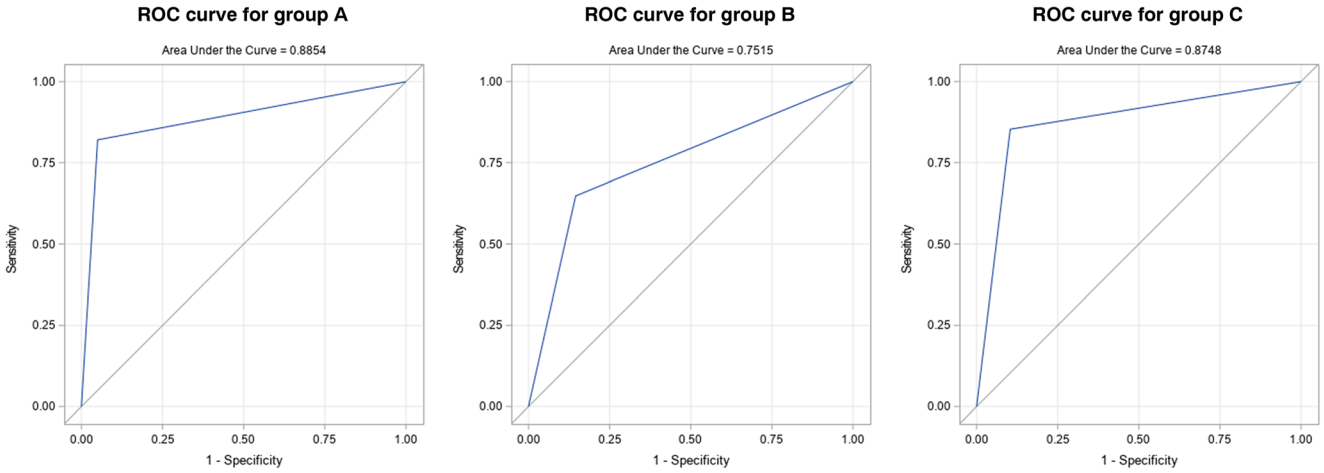

Fig. 4 Receiver operating characteristic (ROC) curve for overall performance for each group by pooling data from all readers

a few cases and mostly used for discerning hyperdense cyst and fat.

Quantitative assessment

Quantitative assessment was only applied to lesions more than 10 mm. AUC and optimal thresholds for IC, NIC, and difference in HU (ΔHU) were calculated. All three parameters performed well in distinguishing enhancing from non-enhancing lesions; however, NIC performs slightly better (Fig. 5a). Optimal thresholds and their respective sensitivity and specificity are shown in Table 4.

IC and ΔHU showed strong correlation. Moreover, NIC and IC were able to differentiate between clear cell RCCs (cRCCs) from other enhancing lesions in our study while ΔHU were not. By using quantitative measurement, subclassification of enhancing type based on histopathology was difficult on DECT (NIC, IC) and SECT (ΔHU). However, on DECT (IC/NIC), separation of cRCC from other enhancing lesions was possible, a threshold of IC = 2.15 and NIC = 0.59 provided sensitivity of 92% and 84.6% respectively. Conversely, ΔHU did not assist in the diagnosis of cRCC (Table 4).

Discussion

Our study confirmed MDI enables confident characterization of renal lesions with high inter-observer concordance in comparison to the conventional renal mass protocol CT (true non-contrast, nephrographic phase and subtraction images). In addition, fewer lesions were misdiagnosed or missed with DECT despite reduced interpretation time. Moreover, iodine quantification is accurate and helpful in further characterizing lesions.

The conundrum of characterizing incidental renal lesions has multiple ramifications on resource utilization, healthcare cost, radiologist's time, and patients' anxiety and morbidity. Guidelines have been introduced to enable management of incidental renal lesions [11]. Since CT is the most frequently used imaging modality for abdominal pathologies, it is desirable to use a single exam that can facilitate renal lesion detection and characterization to provide value-based care without increasing patient's risk [22]. Technological advancements in CT such as scan acquisition, image processing, and reconstruction have addressed these issues to some extent, starting with subtraction CT, and using DECT over time has resulted in further improvement [19, 23–25].

Subtraction techniques have become more feasible with the advent of motion correction registration algorithms, and its clinical applications are emerging [14, 26–29]. Despite excellent results from SCT for detecting subtle contrast in a phantom model [16], these results are not reproduced in our in vivo study, possibly due to misregistration, beam hardening artifacts, and image noise.

Prior studies have demonstrated a high performance of DECT compared to R-CT (sensitivity of 85–100% vs. 70–91.4%, specificity of 85–97% vs. 81–95%, for DECT vs. R-CT) for assessing renal lesions on rsDECT [18, 30–32] and dsDECT [19, 33, 34] platforms, quantitatively and qualitatively. Our results are similar in terms of performance of DECT. However, our study was unique in regard to its large cohort and comparison to SCT. Moreover, we evaluated three readers with varying levels of expertise to measure the reproducibility of results with readers' experience and the impact on interpretation time in comparison to R-CT and SCT. MDI images provide an excellent qualitative representation of enhancement due to nulling of the background soft tissues and minimal pseudo-

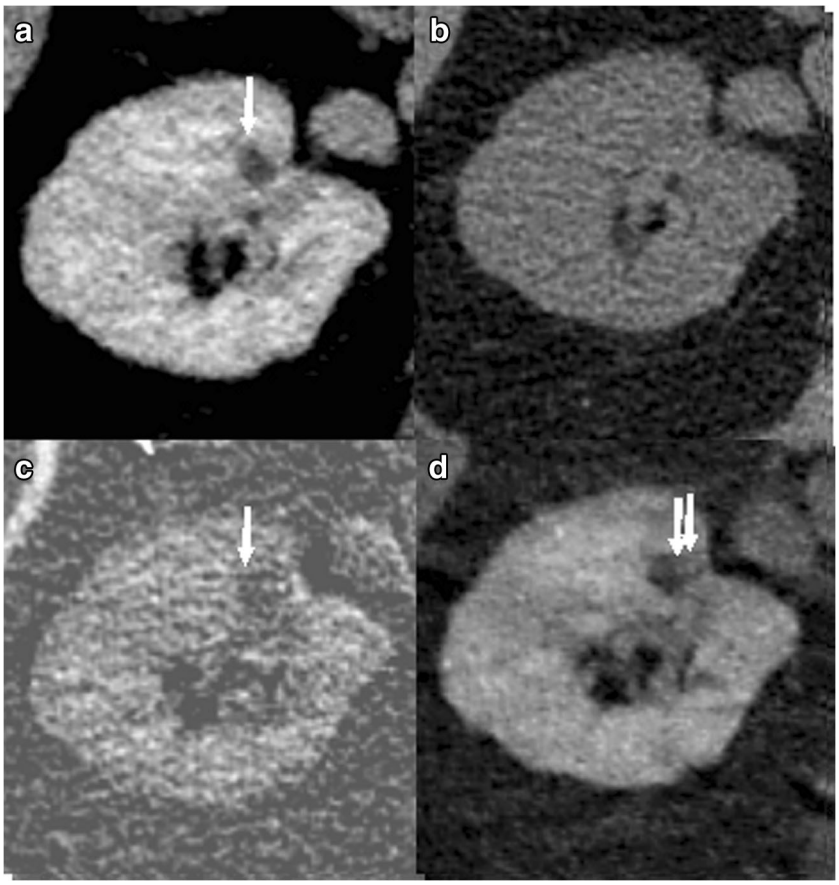

Fig. 5 Nephrographic phase DECT performed in a 55-year-old male with a renal lesion. **a** Virtual monochromatic image at 65 keV, (**b**) true-unenhanced image, and (**c**) subtraction CT show a cystic lesion (arrow) without any discernable worrisome features. However, (**d**) material density iodine (MDI) image demonstrates two enhancing foci along the medial aspect of the lesion (double arrows). Patient subsequently underwent biopsy of the suspected lesion that revealed clear cell carcinoma

enhancement for lesions more than 5 mm [25]. These attributes of MDI were especially valuable in the presence of multiple, hyperdense or smaller lesions (Figs. 5 and 6) which lead to increased efficiency while maintaining high accuracy in our study (Figs. 5 and 6). Another plausible reason for faster interpretation in session 1 was reduced need for quantification. Image reconstructions from a single-phase DECT provides sufficient information for renal lesion characterization. This enables radiation dose reduction compared to a multiphase scan. In our study, the mean $CTDI_{vol}$ for nephrogenic phase was 18.58 mGy which is lower than the American College of Radiology's recommendation for abdominal scans (25 mGy).

IC can be performed on PACS workstation but is rarely applied by our radiologists for interpretation. Using an IC threshold of 1.05 g/cm^3, reliable stratification of enhancing and non-enhancing renal lesions can be made. Recently published phantom experiments also have confirmed the accuracy

Table 4 Quantitative measurement accuracy and corresponding optimal threshold for differentiation of enhancing/non-enhancing lesions and clear cell form of other enhancing lesions

Quantitative measure	Enhancing vs. non-enhancing					Clear cell RCC vs. other enhancing lesions				
	Area under the ROC curve (AUC)	95% confidence interval	Optimal threshold	Sensitivity (%)	Specificity (%)	Area under the ROC curve (AUC)	95% confidence interval	Optimal threshold	Sensitivity (%)	Specificity (%)
Iodine concentration	0.979	0.952–1.000	1.04 mg/ml	95.7	95	0.734	0.592–0.876	2.15 mg/ml	92	57.86
Normalized iodine concentration	0.985	0.974–0.996	0.27	98.6	90	0.723	0.578–0.867	0.59	84	60.52
ΔHU	0.977	0.959–0.994	16.5 HU	95.7	92.5	0.621	0.466–0.777	–	–	–

Note that the ΔHU measurement did not help distinguish clear cell RCC

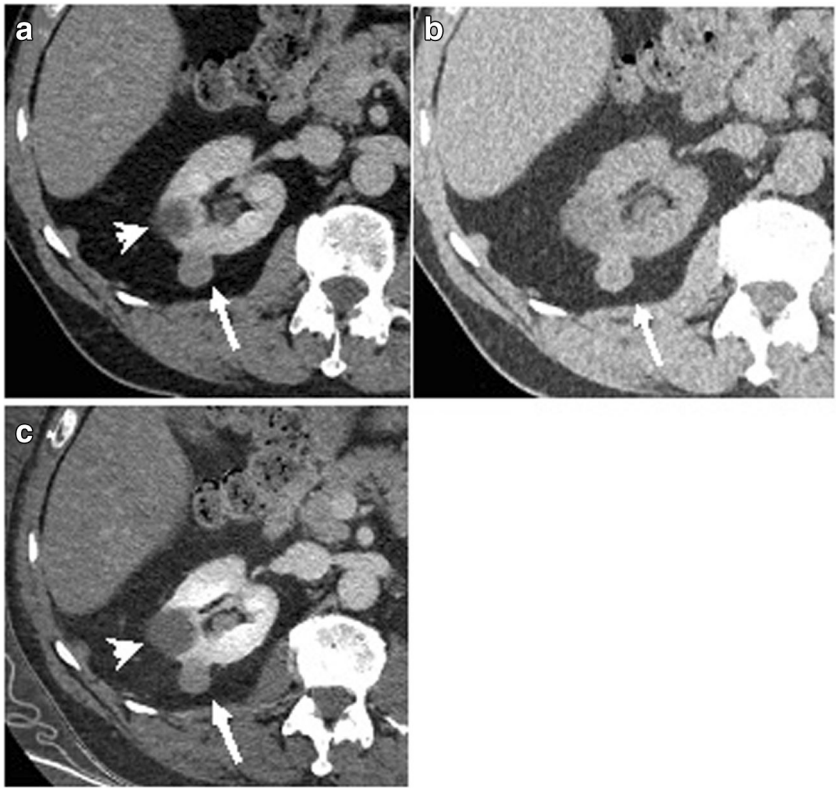

Fig. 6 Nephrographic phase DECT performed in a 68-year-old male with two renal lesions on the right side. Virtual monochromatic image at 65 keV (**a**) demonstrates a 19-mm hyperdense lesion (70 HU) in the posterior aspect (arrow) and a 13-mm cystic lesion (16 HU) with questionable enhancement anteriorly (arrowhead). Conventionally, characterization entails measurement of attenuation on true unenhanced image (**b**), which was 37 HU and 10 HU, respectively, followed by calculation of ΔHU. However, a single series of MDI images (**c**) enables confident and faster characterization of the lesions subjectively. Histopathology of the posterior enhancing lesion revealed papillary renal cell carcinoma

and reproducibility of iodine quantitation across different DECT platforms within a range of 1–10 mg/ml [35–38].

In our study, readers reported infrequent need for MDW images and were only useful for discerning hyperdense cysts and fat-containing lesions. We did not perform measurements on these images. However, if needed, HU can be measured on virtual unenhanced (VUE) image reconstructions from the latest generation of rsDECT and these values have been shown to correlate with TUE images [39–41].

Few lesions were missed on MDI. A possible reason for missed lesions on MDI images was the lack of coronal reformats. These missed lesions in our cohort were small and, at the poles and studies, have shown the superiority of coronal reformats for their evaluation over axial images [42].

This study had a few limitations: first, since this is a retrospective study, we did not ascertain readers' performance on only MDI images in rendering diagnostic interpretation in a clinical setting. However, three readers with variable expertise in this large cohort demonstrated concordant reproducible results supporting the value of MDI images. Moreover, since the time we have introduced DECT in our practice (2010), looking at MDI image datasets has become the preferred method of evaluating renal lesions. Second, we did not have histopathology for all the lesions that were evaluated and relied on a combination of follow-up imaging and clinical data for most of the lesions which is an imperfect but acceptable reference of standard [30, 43], given the logistics of renal lesions which are very common. Third, lesion enhancement measurement on 65-keV images might vary based on a different kVp selection on SECT but HU trend will be similar and they have been shown to closely follow SECT measurements [44]. Fourth, we did not quantitate MDW images as explained before. Finally, we excluded lesions smaller than 5 mm due to concerns for reproducibility of quantitative measurements [45] and lack of reference standard validation.

In conclusion, single-phase DECT enables confident and efficient characterization of renal lesions irrespective of readers' experience, especially in smaller lesions, in comparison to conventional approaches and subtraction CT. These benefits have the potential to reduce radiation dose by obviating the need for additional TUE images, save time by using fewer image datasets that have a high image quality, and decrease cost by reducing the number of additional imaging tests. Quantitatively, IC and NIC were comparable to HU for discerning between enhancing and non-enhancing lesions.

However, they enabled differentiation of clear cell RCC from other enhancing lesions, while HU could not.

Acknowledgements This work was conducted with support from the Harvard Catalyst | The Harvard Clinical and Translational Science Center (National Center for Advancing Translational Sciences, National Institutes of Health Award UL 1TR002541) and financial contributions from Harvard University and its affiliated academic healthcare centers. The content is solely the responsibility of the authors and does not necessarily represent the official views of Harvard Catalyst, Harvard University, and its affiliated academic healthcare centers, or the National Institutes of Health.

Funding The authors state that this work has not received any funding.

Compliance with ethical standards

Guarantor The scientific guarantor of this publication is Dushyant Vasudeo Sahani.

Conflict of interest Dushyant Vasudeo Sahani, MD has the following disclosures which are not relevant to this work: research grant support from GE, Philips, and Bayer Healthcare; royalties (Elsevier); and being a consultant of Allena Pharmaceuticals, GE Healthcare. Other authors have no relevant disclosure. The data was handled by an investigator with no conflict of interest.

Statistics and biometry Hang Lee, Ph.D. kindly provided the statistical advice for this manuscript. One of the authors has significant statistical expertise.

Informed consent Written informed consent was waived by the institutional review board.

Ethical approval Institutional review board approval was obtained.

Methodology
- Retrospective
- diagnostic study
- performed in one institution

References

1. Al Harbi F, Tabatabaeefar L, Jewett MA, Finelli A, O'Malley M, Atri M (2016) Enhancement threshold of small (< 4 cm) solid renal masses on CT. AJR Am J Roentgenol 206:554–558
2. Apfaltrer P, Meyer M, Meier C et al (2012) Contrast-enhanced dual-energy CT of gastrointestinal stromal tumors: is iodine-related attenuation a potential indicator of tumor response? Invest Radiol 47: 65
3. Ascenti G, Mileto A, Krauss B et al (2013) Distinguishing enhancing from nonenhancing renal masses with dual-source dual-energy CT: iodine quantification versus standard enhancement measurements. Eur Radiol 23:2288–2295
4. Baerends E, Oostveen LJ, Smit CT et al (2018) Comparing dual energy CT and subtraction CT on a phantom: which one provides the best contrast in iodine maps for sub-centimetre details? Eur Radiol 28:5051–5059
5. Birnbaum BA, Maki DD, Chakraborty DP, Jacobs JE, Babb JS (2002) Renal cyst pseudoenhancement: evaluation with an anthropomorphic body CT phantom. Radiology 225:83–90
6. Birnbaum BA, Hindman N, Lee J, Babb JS (2007) Multi–detector row CT attenuation measurements: assessment of intra- and interscanner variability with an anthropomorphic body CT phantom. Radiology 242:109–119
7. Borhani AA, Kulzer M, Iranpour N et al (2017) Comparison of true unenhanced and virtual unenhanced (VUE) attenuation values in abdominopelvic single-source rapid kilovoltage-switching spectral CT. Abdom Radiol (NY) 42:710–717
8. Cha D, Kim CK, Park JJ, Park BK (2016) Evaluation of hyperdense renal lesions incidentally detected on single-phase post-contrast CT using dual-energy CT. Br J Radiol 89:20150860
9. Chandarana H, Megibow AJ, Cohen BA et al (2011) Iodine quantification with dual-energy CT: phantom study and preliminary experience with renal masses. AJR Am J Roentgenol 196:W693–W700
10. Chandler A, Wei W, Herron DH, Anderson EF, Johnson VE, Ng CS (2011) Semiautomated motion correction of tumors in lung CT-perfusion studies. Acad Radiol 18:286–293
11. Chandler A, Wei W, Anderson EF, Herron DH, Ye Z, Ng CS (2012) Validation of motion correction techniques for liver CT perfusion studies. Br J Radiol 85:e514–e522
12. Dillman JR, Caoili EM, Cohan RH, Ellis JH, Francis IR, Schipper MJ (2008) Detection of upper tract urothelial neoplasms: sensitivity of axial, coronal reformatted, and curved-planar reformatted image-types utilizing 16-row multi-detector CT urography. Abdom Imaging 33:707–716
13. Ding A, Eisenberg JD, Pandharipande PV (2011) The economic burden of incidentally detected findings. Radiol Clin North Am 49:257–265
14. Eisner B, Kambadakone A, Samir A, Sahani D (2010) 619 subtraction ct improves radiologist confidence in evaluation of enhancing renal lesions. J Urol 183:e243–e244
15. Feuerlein S, Heye TJ, Bashir MR, Boll DT (2012) Iodine quantification using dual-energy multidetector computed tomography imaging: phantom study assessing the impact of iterative reconstruction schemes and patient habitus on accuracy. Invest Radiol 47:656
16. Goodsitt MM, Christodoulou EG, Larson SC (2011) Accuracies of the synthesized monochromatic CT numbers and effective atomic numbers obtained with a rapid kVp switching dual energy CT scanner. Med Phys 38:2222–2232
17. Graser A, Johnson TR, Hecht EM et al (2009) Dual-energy CT in patients suspected of having renal masses: can virtual nonenhanced images replace true nonenhanced images? Radiology 252:433–440
18. Graser A, Becker CR, Staehler M et al (2010) Single-phase dual-energy CT allows for characterization of renal masses as benign or malignant. Invest Radiol 45:399
19. Herts BR, Silverman SG, Hindman NM et al (2018) Management of the incidental renal mass on CT: a white paper of the ACR Incidental Findings Committee. J Am Coll Radiol 15:264–273
20. Hock LM, Lynch J, Balaji KC (2002) Increasing incidence of all stages of kidney cancer in the last 2 decades in the United States: an analysis of surveillance, epidemiology and end results program data. J Urol 167:57–60
21. Hollingsworth JM, Miller DC, Daignault S, Hollenbeck BK (2006) Rising incidence of small renal masses: a need to reassess treatment effect. J Natl Cancer Inst 98:1331–1334
22. Jamis-Dow CA, Choyke PL, Jennings SB, Linehan WM, Thakore KN, Walther MM (1996) Small (< or = 3-cm) renal masses: detection with CT versus US and pathologic correlation. Radiology 198: 785–788
23. Jayson M, Sanders H (1998) Increased incidence of serendipitously discovered renal cell carcinoma. Urology 51:203–205
24. Jinzaki M, Tanimoto A, Mukai M et al (2000) Double-phase helical CT of small renal parenchymal neoplasms: correlation with pathologic findings and tumor angiogenesis. J Comput Assist Tomogr 24:835

25. Kambadakone A, Arasu VA, Samir AE et al (2012) Qualitative assessment of enhancement in a renal mass: contribution of subtraction CT. J Comput Assist Tomogr 36:381
26. Kaza RK, Caoili EM, Cohan RH, Platt JF (2011) Distinguishing enhancing from nonenhancing renal lesions with fast kilovoltage-switching dual-energy CT. AJR Am J Roentgenol 197:1375–1381
27. Koonce JD, Vliegenthart R, Schoepf UJ et al (2014) Accuracy of dual-energy computed tomography for the measurement of iodine concentration using cardiac CT protocols: validation in a phantom model. Eur Radiol 24:512–518
28. Mahmood U, Horvat N, Horvat JV et al (2018) Rapid switching kVp dual energy CT: value of reconstructed dual energy CT images and organ dose assessment in multiphasic liver CT exams. Eur J Radiol 102:102–108
29. Manoharan D, Sharma S, Das CJ, Kumar R, Singh G, Kumar P (2018) Single-acquisition triple-bolus dual-energy CT protocol for comprehensive evaluation of renal masses: a single-center randomized noninferiority trial. AJR Am J Roentgenol 211:W1–W11
30. Marin D, Davis D, Roy Choudhury K et al (2017) Characterization of small focal renal lesions: diagnostic accuracy with single-phase contrast-enhanced dual-energy CT with material attenuation analysis compared with conventional attenuation measurements. Radiology 284:737–747
31. Matsumoto K, Jinzaki M, Tanami Y, Ueno A, Yamada M, Kuribayashi S (2011) Virtual monochromatic spectral imaging with fast kilovoltage switching: improved image quality as compared with that obtained with conventional 120-kVp CT. Radiology 259:257–262
32. McCarthy CJ, Baliyan V, Kordbacheh H, Sajjad Z, Sahani D, Kambadakone A (2016) Radiology of renal stone disease. Int J Surg 36:638–646
33. Mileto A, Nelson RC, Samei E et al (2014) Impact of dual-energy multi–detector row CT with virtual monochromatic imaging on renal cyst pseudoenhancement: in vitro and in vivo study. Radiology 272:767–776
34. Mileto A, Marin D, Ramirez-Giraldo et al (2014b) Accuracy of contrast-enhanced dual-energy MDCT for the assessment of iodine uptake in renal lesions. AJR Am J Roentgenol 202:W466–W474
35. Mohr B, Brink M, Oostveen LJ, Schuijf JD, Prokop M (2016) Lung iodine mapping by subtraction with image registration allowing for tissue sliding. Proc. SPIE 9784, Medical Imaging 2016: Image Processing, 978442
36. Patel BN, Bibbey A, Choudhury KR, Leder RA, Nelson RC, Marin D (2017) Characterization of small (< 4 cm) focal renal lesions: diagnostic accuracy of spectral analysis using single-phase contrast-enhanced dual-energy CT. AJR Am J Roentgenol 209:815–825
37. Pelgrim GJ, van Hamersvelt RW, Willemink MJ et al (2017) Accuracy of iodine quantification using dual energy CT in latest generation dual source and dual layer CT. Eur Radiol 27:3904–3912
38. Porter ME (2010) What is value in health care? N Engl J Med 363: 2477–2481
39. Savci G, Yazici Z, Sahin N, Akgöz S, Tuncel E (2006) Value of chemical shift subtraction MRI in characterization of adrenal masses. AJR Am J Roentgenol 186:130–135
40. Siegel CL, Fisher AJ, Bennett HF (1999) Interobserver variability in determining enhancement of renal masses on helical CT. AJR Am J Roentgenol 172:1207–1212
41. Tada S, Yamagishi J, Kobayashi H, Hata Y, Kobari T (1983) The incidence of simple renal cyst by computed tomography. Clin Radiol 34:437–439
42. Vasudevan A, Davies RJ, Shannon BA, Cohen RJ (2006) Incidental renal tumours: the frequency of benign lesions and the role of preoperative core biopsy. BJU Int 97:946–949
43. Yoshioka K, Tanaka R, Takagi H et al (2016) Diagnostic accuracy of a modified subtraction coronary CT angiography method with short breath-holding time: a feasibility study. Br J Radiol 89: 20160489
44. Yu L, Christner JA, Leng S, Wang J, Fletcher JG, McCollough CH (2011) Virtual monochromatic imaging in dual-source dual-energy CT: radiation dose and image quality. Med Phys 38: 6371–6379
45. Zarzour JG, Milner D, Valentin R et al (2017) Quantitative iodine content threshold for discrimination of renal cell carcinomas using rapid kV-switching dual-energy CT. Abdom Radiol (NY) 42:727–734